INFLUENCE OF TEMPERATURE EFFECTS ON THE SHOCK WAVE/BOUNDARY LAYER INTERACTION OF A SCRAMJET-INLET

T. Neuenhahn, H. Olivier
Shock Wave Laboratory, RWTH Aachen University, 52056 Aachen, Germany

Abstract

The investigation of a scramjet intake in the hypersonic shock tunnel TH2 with special focus on the shock wave/boundary layer interaction (SWBLI) at the kink of the outer compression ramps has been undertaken. The effect of installed or omitted side walls on the outer compression showed that side walls prevent side flow as expected, but add additional heat loads and introduce a complex three-dimensional flow field even for the employed two-dimensional compression ramp shape. To analyse wall temperature effects, the model heating technique has been improved from 840 K to 1000 K simulated wall temperature. The obtained results for the SWBLI's separation length indicate the well known trend of increased separation length for increased wall temperature for constant total or free stream temperature and the not well known trend of a decreased separation length for increased total temperature for constant wall temperature ratio. Beneath the separation length more flow field details have been studied employing static pressure and heat flux measurements by thermocouples and infrared (IR) imaging as well as black-and-white-schlieren and colour schlieren optics.

1. INTRODUCTION

The current interest in scramjet propulsion for future launcher applications and others tasks has drastically increased due to the first successful flight tests. As part of Germany's scramjet research the research training group (GRK) 1095/1 "Aero-Thermodynamic Design of a Scramjet Propulsion System for Future Space Transportation Systems" studies a scramjet propulsion system with experimental, numerical and analytical means as well as the conceptional point of view is considered[1,2,3]. The regarding research at the Shock Wave Laboratory investigates the inlet flow field which is often divided in an outer and inner compression. For the outer compression geometrical means like e.g. compression ramps are employed to increase the static pressure and static temperature for an efficient thermodynamic cycle of the combustion process. The inner compression is a result of the combustion pressure rise which acts upstream through the subsonic part of the boundary layer and can unstart the inlet, if the pressure rise reaches the inlet throat. The designed and build scramjet inlet model has been developed to analyse the outer and inner compression, whereas the outer compression has been investigated in the first funding period of the GRK and the inner compression will be studied in the next funding period (2008 to 2010).

The flow field of the outer compression is mainly influenced by SWBLIs occurring at the kink of two compression ramps or at the cowl shock impingement which change the aerodynamic force, the heat load, the inlet's total pressure loss and the captured mass flow thus changing the inlet performance. In previous studies[4,5] we have employed a double ramp model which ensures two-dimensional flow in the midspan of the model to investigate different effects on the separation length and other features of the regarding SWBLI by experiment and CFD calculations. The considered effects included the effect of elevated wall temperature, leading edge bluntness and boundary layer transition upstream, downstream and in the SWBLI.

The investigated scramjet inlet flow field could no longer be treated as two-dimensional due to the influence of side walls and the regarding corner flow between the side walls and the compression ramp geometry. The omission of the side walls reduces the skin friction drag due to the reduced wetted area, but allows flow spillage over the model sides thus decreases the captured mass flow. Due to the advantages and disadvantages of the inlet with and without side wall both configurations have been investigated. Moreover, the effect of total temperature on the SWBLI length is looked after, as the total temperature effect on a laminar compressible boundary layer is known[6] thus there should be also an effect on SWBLI.

2. EXPERIMENTAL SETUP

2.1. Hypersonic shock tunnel TH2

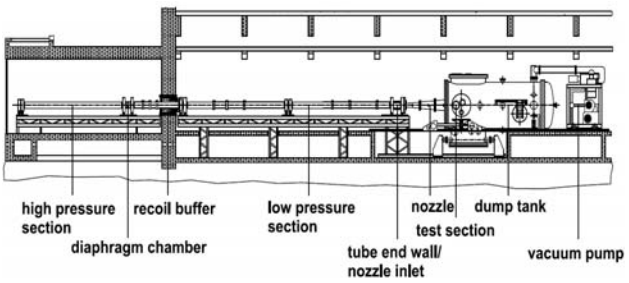

Fig. 1: Basic setup of the shock tunnel TH2 for helium-driven mode

The hypersonic shock tunnel TH2 (Fig. 1) working in helium-driven mode has been employed for the current research. The tunnel can simulate re-entry flow conditions with total enthalpies from 1.5 to 14.6 MJ/kg and Mach

numbers from 6.6 to 14 using helium-driven or detonation-driven mode[7,8].

The free-stream conditions for the performed experiments are given with respect to the model's leading edge in TAB. 1. The slender conical nozzle with a small half apex angle of 5.8° creates small axial gradient of the free-stream conditions in the test section[9]. These are taken into account by the determination of the pressure coefficient (equation (1)) and the Stanton number (equation (2)).

(1) $$c_p = \frac{p - p_\infty}{0.5\rho_\infty u_\infty^2}$$

(2) $$C_H = \frac{\dot{q}}{\rho_\infty u_\infty (h_0 - h_W)}$$

TAB. 1: TH2 free-stream conditions

	Cond. I	Cond. II
Ma_∞ [-]	7.7	7.6
Re_∞ [1/m]	$3.5 \cdot 10^6$	$4.5 \cdot 10^6$
T_0 [K]	1300	2200
T_∞[K]	100	210

The two flow conditions feature similar free-stream Mach and unity Reynolds numbers and differ only in the total temperature and the free-stream temperature. Therefore, that beneath the Mach and Reynolds number the wall-to-free-stream ratio is a similarity parameter for a laminar boundary layer, the wall temperature must be adjusted to investigate only the total temperature effect on the flow field.

2.2. Heated intake model

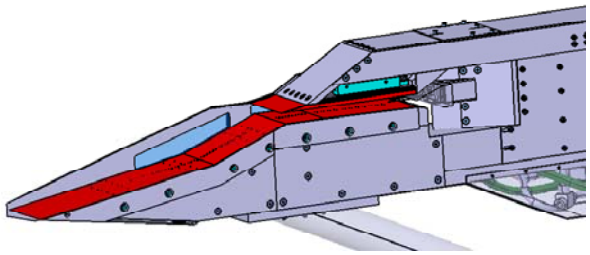

Fig. 2: Heated intake model without left sidewall

A digital mock-up of the scramjet intake model with only the right side wall mounted is given in Fig. 2 and the dimensions of the investigated compression ramps with following horizontal isolator part are shown in Fig. 3. The width of the model is 0.1 m. For the experiments without side walls the width-to-first-ramp-length-ratio B/L_I is an important criterion for the evaluation, if the SWBLI could be treated as two-dimensional. The ratio of this model is 0.37 thus being smaller than the value proposed by Lewis and Kubota[10] of 1 so that three-dimensional effects on the SWBLI are expected. The model side walls are equipped with windows which allow optical access of the SWBLI at the compression corner kink and the isolator flow field also for the installed side walls.

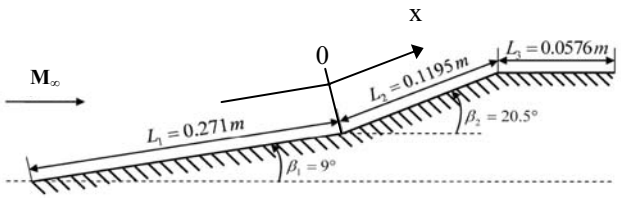

Fig. 3: Two-dimensional sketch of the model

2.3. Model heating technique

The surface temperatures of the model ramp geometry and the cowl plate are elevated by nine resistance heating elements to simulate different wall temperatures between 300 K and 1000 K. The temperature distributions along the first two ramps for different simulated wall temperatures are given in Fig. 4. Moreover, at three positions along the surface (x/L_I = -0.56, -0.08 and 0.32) five measurements in lateral directions have been taken which indicate including the longitudinal measurements that the variation of the simulated surface temperature is less than 10% for the whole flow wetted area.

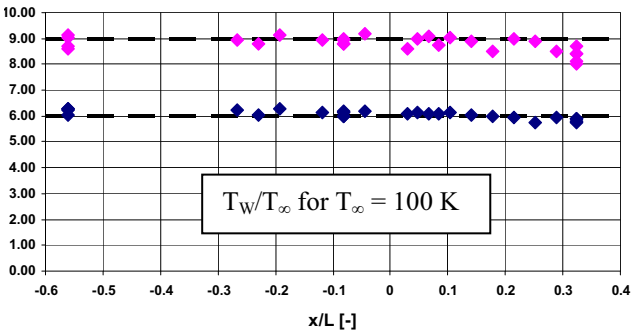

Fig. 4: Surface temperature distribution for different simulated wall temperatures

Beside the heating of the model's flow wetted surfaces the model heating technique includes a special thermal insulation technique which ensures a uniform wall temperature distribution in streamwise and lateral direction. Moreover, this technique determines for the installed heating power the highest achievable wall temperature. The thermal insulation is needed because the employed cylindrical pressure transducers with a diameter of only 2 mm allow high spatial resolution of the flow field, but require room temperature environment thus being water cooled. Moreover, due to the short measurement times of a shock tunnel the pressure transducer have to be installed close to the surface. To prevent the high heat loss due to the short distance and the large temperature difference between the heated ramp plate and the cold water cooler a sandwich construction as

thermal insulation is employed (Fig. 5). The sandwich construction consists of five polished stainless steel plates which are separated by ceramic washers. The convective heat flux is reduced due to the low heat conductivity of the ceramic washer material. Heat radiation is decreased due to the five layers of polished stainless steel having a low emission coefficient being smaller than 0.1. Heat convection could be neglected as the test section with the model is evacuated prior to the experiment. For the simulated wall temperature case of 1000 K this leads to a temperature gradient of 875 K/cm.

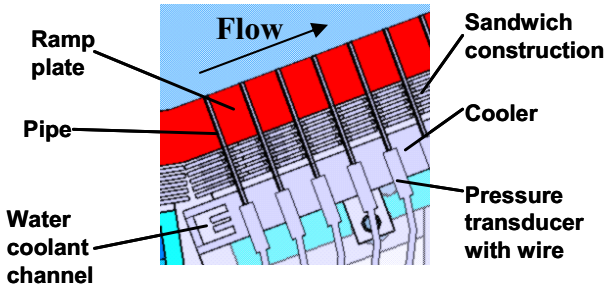

Fig. 5: Cross-section view of the pressure transducer installation and isolation sandwich device

2.4. Measurement techniques

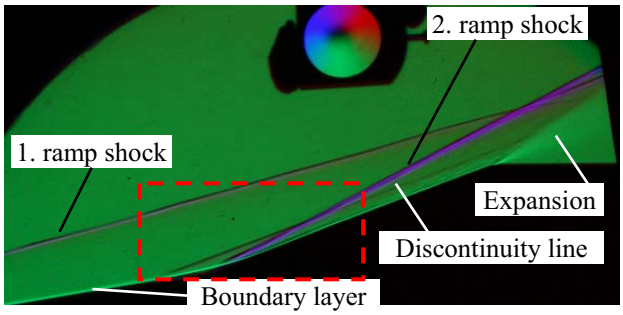

Fig. 6: Colour schlieren image, reference case

The employed measurement techniques are wall pressure and heat flux measurement by thermocouples and IR imaging. The IR imaging and the schlieren imaging visualize the spatial distributions of the heat load of the wetted surfaces and the density gradient distribution in the plane normal to the ramp geometry. The model is equipped with 39 Kulite piezo-resistive sensors for wall pressure measurements and 32 self-made type E coaxial thermocouples for heat flux measurements[11]. The IR imaging determines the temperatures during the experiments which allow heat flux measurements in line scan mode (2x256 Pixel) and temperature distributions of the full image (320x256 Pixel) being the result of the heat load of the flow. The colour scale of the IR images is adjusted to visualise the flow features and is different for the Figs. 11, 18 and 22. The schlieren optic has been employed in different configurations. The colour schlieren image (Fig. 6) indicating the direction of the density gradients for a better interpretation of the flow field. The colour mask in the upper portion of Fig. 6 decodes the direction of the density gradients. The black-and-white-schlieren-images (Fig. 15) feature the advantage that the displayed density gradient range is known by the setup of the schlieren system and the relation between the displayed brightness change and the measured density gradient is linear. The displayed density gradients of the shown schlieren images are in the range of ±75 kg/m^4, whereas grey indicates no density gradient.

3. EXPERIMENTAL RESULTS

The flow field without side wall and a cold wall (T_W = 300 K) is shown in Fig. 6 displaying the first ramp shock, the developing boundary layer on the first ramp which interacts with the second ramp shock in the SWBLI at the ramps' kink (Fig. 7).

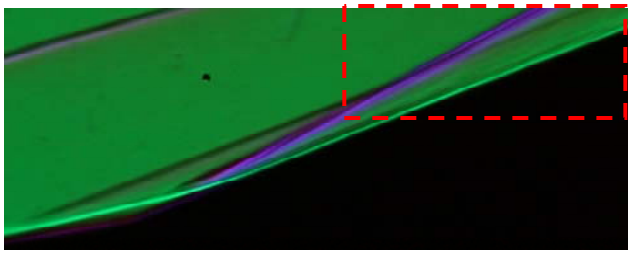

Fig. 7: Zoomed image of Fig. 6: SWBLI

Downstream of the SWBLI the discontinuity line is clearly visible separating the streamlines processed only by the first and second ramp shock above the discontinuity line and the streamlines passed the first ramp shock and the SWBLI. The latter stream lines form the distorted flow field displaying not a clear boundary layer edge (Fig. 8). Due to the expansion at the end of the second ramp the distorted flow vanishes (Fig. 6).

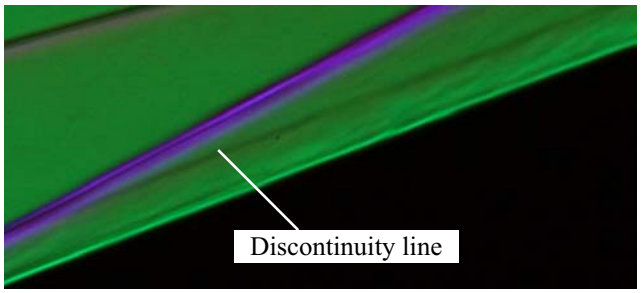

Fig. 8: Zoomed image of Fig. 7: Downstream of the SWBLI

3.1. Reference case

The colour schlieren images (Figs. 6, 7 and 8) are obtained for flow condition I, a cold wall and without side walls. This case is called the reference case. The above described flow field features have been observed for different total temperatures and wall temperatures thus they describe general features for the undertaken research. The difference between the case with to the case without side walls are described later. The pressure distribution along the first two ramps of three experiments indicate the good reproducibility. The pressure measurements agree with inviscid theory upstream $c_{p,I}$ and downstream $c_{p,III}$ of the interaction and with the plateau pressure $c_{p,II}$ of the free interaction theory by Chapman[12].

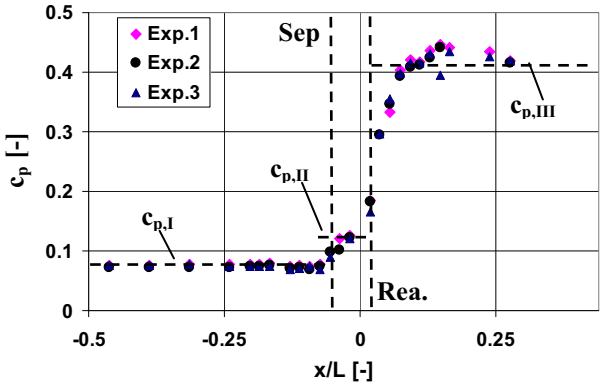

Fig. 9: Pressure distribution for the reference case

The Stanton number distribution (Fig. 10) indicates a laminar flow due to the agreement with the Van Driest solution[13] for the laminar boundary layer and a laminar separation due to the decreasing heat flux in the separated region. The high heat fluxes at reattachment measured by the thermocouple agree with the IR line scan at the lateral position of 19.4 mm from the midspan of the model. The IR line scan at 4.8 mm indicates a lower level but the heat flux increases with the running length until it reaches the level of the 19.4 mm lateral position ($x/L_l \approx 0.3$). For the two investigated experiments there is a large deviation between the second but last thermocouple measurement and moreover the IR line scan decreases to a laminar level with further running length where as the last thermocouple measurement indicate an increasing heat flux to a turbulent level.

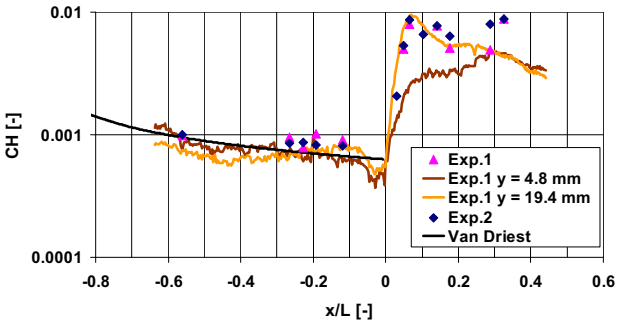

Fig. 10: Stanton number distribution for the reference case

The difference between the thermocouple measurement and IR line scans is explained by the IR image (Fig. 11). The black circles indicate the thermocouple positions which have been left out by the black painting for the infrared imaging. The first ramp indicates clearly the separation line due to the decreased temperature. Downstream of the kink the reattachment line is marked by the upstream edge of the Goertler vortices' footprint. These counterrotating vortices cause alternating high and low heat loads in lateral direction. This explains the different heat loads of the IR line scans downstream of reattachment – in the so called Goertler zone. Moreover, the direction of the Goertler vortices' footprint turns to sides indicating the side flow.

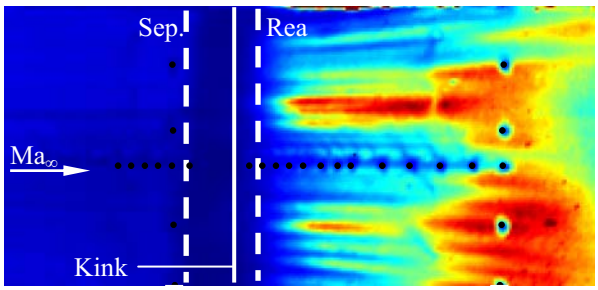

Fig. 11: IR image of the reference case

Downstream of this Goertler zone the heat flux rises or decreases depending on the lateral position. This behaviour might be described by the model of Kreins[14] who investigated a SWBLI due to an impinging shock wave on a hypersonic flat plate boundary layer. Due to heat flux and Pitot pressure measurements, he developed a model for the flow field downstream of the Goertler zone (Fig. 12). The Goertler vortices break down after a certain distance and a new, vortex-free sublayer develops which has a distorted edge flow. This distorted edge flow could lead to bypass transition which would explain the turbulent heating levels. Moreover, the flow expands from the high reattachment pressure to the inviscid second ramp pressure shown by the pressure decrease in Fig. 9 having a stabilizing effect on the boundary layer thus preventing bypass transition.

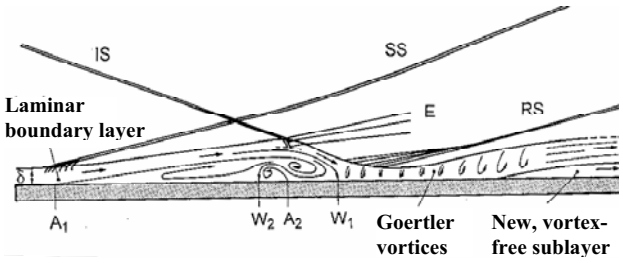

Fig. 12: Sketch of a SWBLI with downstream flow field[14], IS: incipient shock, SS: separation shock, E: expansion, RS: reattachment shock

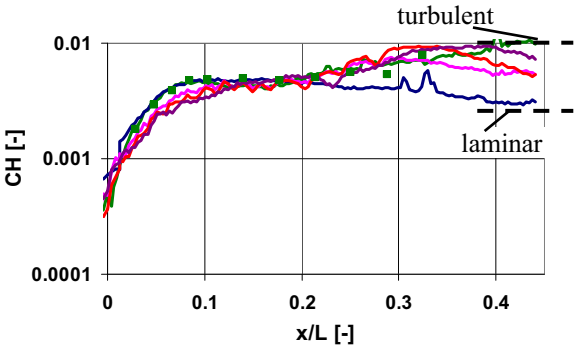

Fig. 13: Stanton number distribution of the second ramp for different experiments of the reference case, symbols: thermocouples measurements, solid: lines IR-thermography

Further experiments for the reference case showed different heat fluxes downstream of the Goertler zone spanning from pure laminar over transitional to turbulent heat flux levels (Fig. 13) indicating a non-sharp border between the laminar and turbulent regime.

3.2. Wall temperature influence

The wall temperature effect is only shown briefly being discussed more detailed elsewhere[4,5]. It has no effect on the measured pressure distribution upstream of the SWBLI. For constant total temperature the separation size is increased with increasing wall temperature which is by the shown scale only visible by the schlieren results. The maximum reattachment pressure is reduced. The larger separation size is a result of the thicker boundary layer due to the higher wall temperature. This increased thickness reduces the velocity gradient at the wall and with it the shear stress. Due to the force balance of the upstream acting pressure of the second ramp shock and the shear stress the separation point travels upstream and increases the separation size.

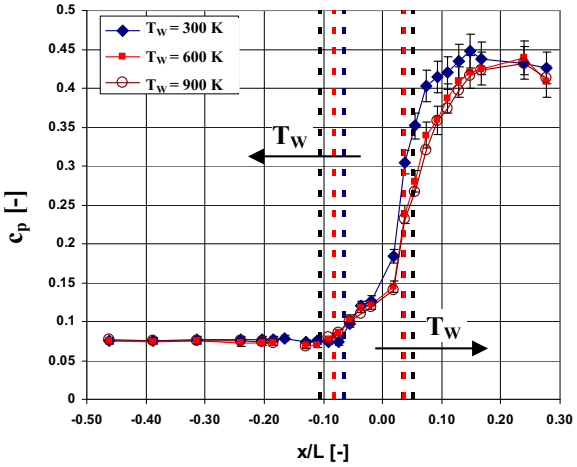

Fig. 14: Pressure distribution for different wall temperatures, Cond. I

3.3. Sidewall influence

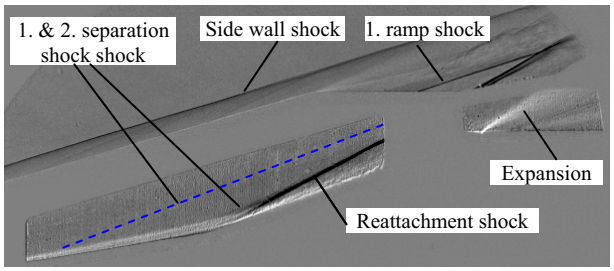

Fig. 15: Schlieren image with installed side wall, Cond. I

The schlieren image of the case with side wall allows to investigate the flow field through the two window sections and above the side wall. The cowl plate has been omitted to have a better comparison to the reference case. The image indicates a shock wave due to the side wall installation, the first ramp shock mainly covered by the side wall, two separation shocks and one reattachment shock of the SWBLI and an expansion fan downstream of the second ramp (Fig. 15). The image quality is slightly decreased due to the installed two additional window pairs, but still give a good insight in the flow field details. For comparison with the black-and-white-schlieren image the colour schlieren image is given in Fig. 16.

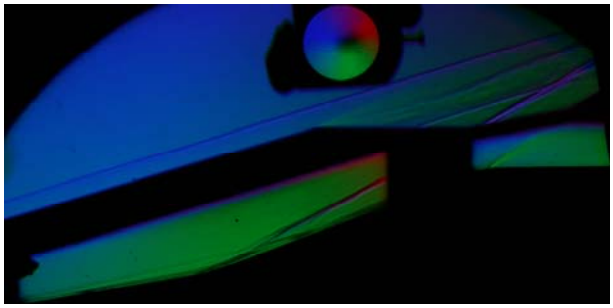

Fig. 16: Colour schlieren image with installed side walls, Cond. I

For the side wall case the layer close to the wall and upstream of the SWBLI is thicker than the visible layer in Fig. 6. In this figure the visible layer represents the boundary layer, but in the case with installed side walls the boundary layer and the corner flow are superimposed thus the corner flow has more than double the height of the boundary layer. Moreover, the more upstream separation shock is hardly visible so that it is indicated by a dashed line. The second separation shock is close to the kink and mainly hidden by the corner flow. Downstream of the reattachment shock no clear discontinuity line is visible due to the missing of a defined triple point of the separation, reattachment and resulting second ramp shock.

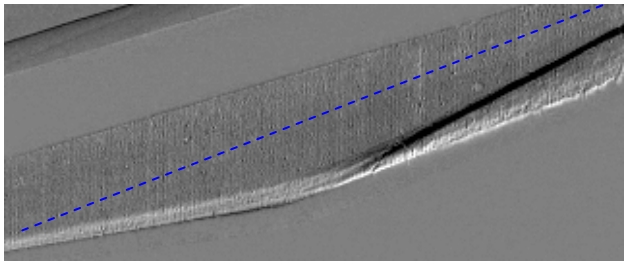

Fig. 17: Zoomed image of Fig. 15: SWBLI

To explain the occurrence of two separation shocks with one hardly visible, the IR image (Fig. 18) is employed. Upstream of the interaction the heating due to the corner flow is clearly visible. The separation line has a kind of a tongue form. The more downstream position of the separation in the regions of the corner flow is a result of the corner flow which transports high energetic flow to the ramp wall. This causes the increased heat load and energizes the boundary layer to withstand the upstream acting pressure thus leading to a smaller separation size at these lateral positions. The separation position in the model midspan is increased compared to the reference case due to the prevented side flow by the side walls. Concluding, in the lateral direction the first ramp can be classed in the corner flow influenced parts and the corner uninfluenced part with regarding separation position and separation shock. The schlieren image compresses this information over the flow field depth thus the tongue form separation shock line appears as two shocks. Due to the small span of the corner flow uninfluenced part in the model midspan and therefore the small light deflection, this shock is hardly visible. The separation shock of the corner flow influenced parts appear stronger due to their larger span compared to the midspan part. In addition, the pressure rise in the midspan is slower thus creating compression waves instead of a separation shock which

also cause a reduced light deflection. However, the findings of the separation line's tongue form is confirmed by the lateral distributed thermocouples upstream of the kink (x/L_l = -0.08, marked in Fig. 11).

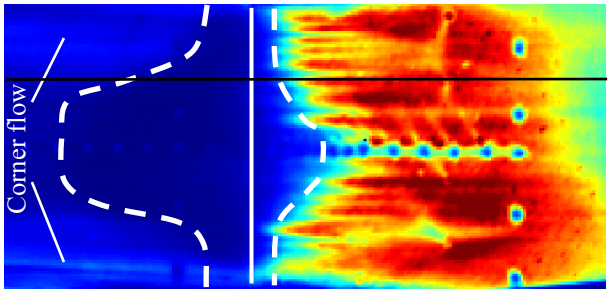

Fig. 18: IR image of the flow field with side walls, black line: line scan position of Fig. 20

The reattachment line is marked by the upstream edge of the Goertler vortices' footprints and is representative of the form of the separation line. The Goertler vortices' distribution appears to be more regular with similar peak heating values compared to the reference case. Also the number of vortices' footprints is increased thus the vortex's diameter is decreased. The flow field downstream of the Goertler vortices breakdown shows the same behaviour as the reference case.

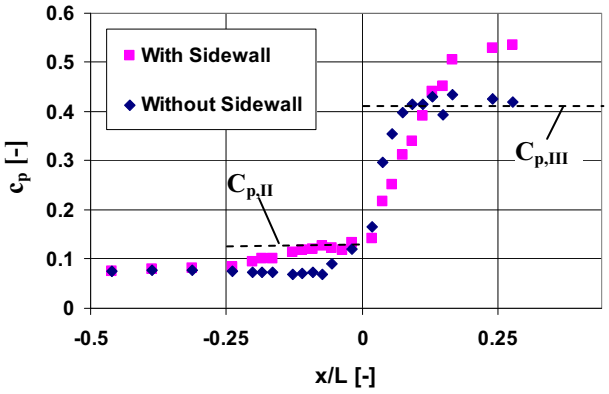

Fig. 19: Pressure distribution with and without sidewall

The pressure distribution along the midspan of the model indicates the corner flow undisturbed behaviour with a larger separation than the reference case (Fig. 19). The separation position of the reference case is further upstream than of the corner flow influenced part thus the corner flow energizes the boundary layer upstream of the SWBLI more than the side flow. Both cases reach a similar plateau pressure $c_{p,II}$ but the pressure rise is higher for the case with side walls preventing side flow. This is also observed by the comparison of the Goertler vortices' footprints in the IR images (Fig. 11 and Fig. 18) which are oriented in streamwise direction for the installed side walls.

The Stanton number distribution also indicates a larger separation in the midspan of the model (Fig. 20). The increased wall pressure downstream of the reattachment corresponds to higher static temperatures which would lead to higher heat loads. Due to the increased separation size the reattachment process is spread over a wider distance reducing the heat load so that both effects for higher and lower heat fluxes compensate each other and similar reattachment heat fluxes are obtained. For the case with side walls the thermocouple measurements and the IR line scan show different separation poitions indicated by the rapid heat flux decrease. The shown line scan's position is offset from the midspan thus indicating the separation position between the corner uninfluenced and corner influenced part. The line scan of Fig. 20 and the IR image of Fig. 18 have been obtained for different experiments thus the heat flux downstream of the Goertler zone decreases for the IR image and stays constant for the line scan. This behaviour of laminar or turbulent flow downstream of the Goertler zone is described for the reference case (Fig. 13).

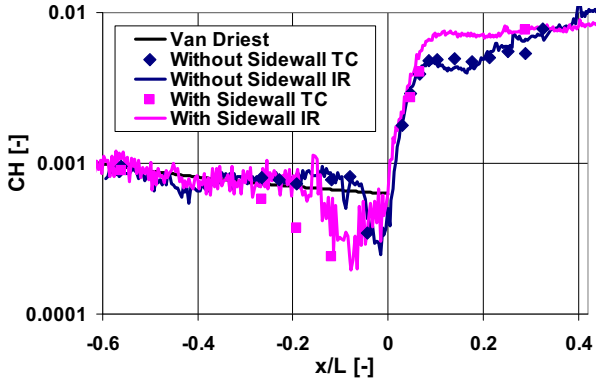

Fig. 20: Stanton number distribution with and without sidewall

3.4. Total temperature influence

To investigate the total temperature effect on the flow field all other flow similarity parameters must be unchanged. The two chosen flow conditions of our hypersonic shock tunnel TH2 feature the same free stream Mach number and nearly the same unit Reynolds number thus fulfilling this criterion for these similarity parameters. Due to the different total temperatures and the free-stream-to-total-temperature-ratio given by the Mach number the free stream temperature is also different thus for unchanged wall temperature the wall-to-free stream-temperature ratio would be changed. The analytical solution for the compressible boundary layer equations by Van Driest[13] indicates an influence of this ratio on the boundary layer profile. To also exclude this effect on the flow field, the wall temperature is rised for the higher total temperature case so that the wall-to-free-stream-temperature ratio is constant.

For the model with mounted side walls the pressure distribution (Fig. 21) indicates a smaller separation length for the increased total temperature. As in the comparison with and without side walls the plateau pressure remains unchanged.

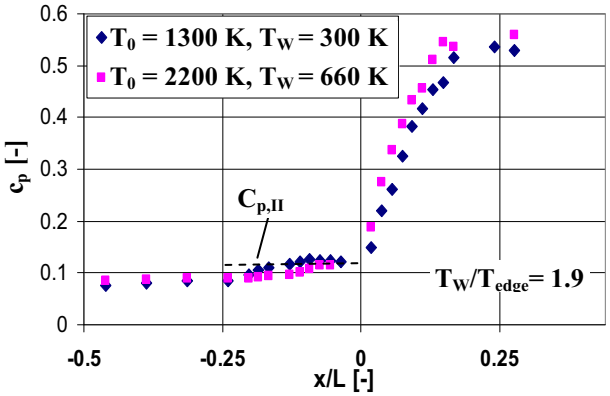

Fig. 21: Pressure distribution for different total temperatures and constant TW/Tedge of 1.9

The IR image for the increased total temperatures (Fig. 22) shows that the reattachment line is close to the kink line confirming the above findings of a reduced separation length (Fig. 18). The separation line is not visible due to the reduced image quality as a result of the elevated wall temperature. The increased heat flux due to the corner flow is still visible indicating some asymmetry which is also recognized in the reattachment line. Currently, there is no explanation for the asymmetry, as zero degree yaw angle and the rectangular inclination of the side walls with respect to the ramp geometry have been checked carefully. However, the observed relation that an energized boundary layer indicated by the increased heat load upstream of the kink leads to a smaller separation size is confirmed.

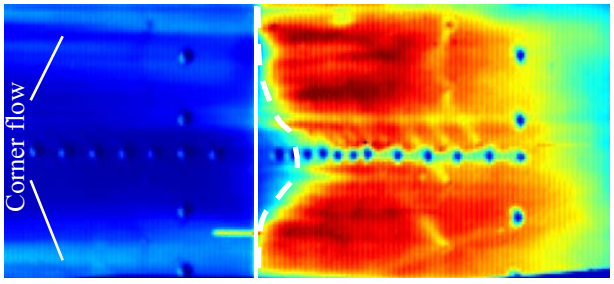

Fig. 22: IR image for increased total temperature

The reason for the decreased separation length for increased total temperature is the increased temperature level in the boundary layer and with it an increased mean viscosity being a function of temperature. The increased temperature level can be explained with the reference temperature method by Eckert[15]. This method employs a reference temperature to transfer the Blasius solution for the incompressible boundary layer to the compressible boundary layer. This reference temperature (equation 3) is determined with respect to the wall temperature T_W, the adiabatic wall temperature T_{aw} and the boundary layer edge temperature T_e so that the transferred Blasius profile matches the compressible profile.

$$T_{ref} = 0.28 \cdot T_e + 0.5 \cdot T_W + 0.22 \cdot T_{aw} \quad (3)$$

For the higher total temperature case the reference temperature and with it the viscosity level is increased and therewith the shear stresses in the boundary layer. These stresses are in balance with the pressure gradient induced by the shock wave causing the SWBLI, as stated by the free interaction theory[12]. Thus, increasing the shear stress creates an imbalance forcing the separation point downstream. Due to the fact that the shear stress in a boundary layer decreases with running length, the separation position is pushed downstream until a new force balance of the shear stresses with the unchanged pressure gradient is reached.

4. CONCLUSION

The undertaken research investigates the flow field of a scramjet inlet with special focus on the shock wave/boundary layer interaction at the kink of the two compression ramps. The experimental campaign employs different measurement techniques to obtain

- pressure distributions,
- heat flux distributions,
- black-and-white schlieren images,
- colour schlieren images and
- infrared images.

These observations allowed a detailed investigation of the effects of

- side walls,
- wall temperature and
- total temperature

on the outer compression.

The flow field with omitted side walls showed clearly the effect of side flow leading to a smaller separation length of the SWBLI compared to the case with installed side walls. The observations concerning the side wall installation indicated a complex three-dimensional flow field with increased heat loads due to the corner flow between the side walls and the compression ramp geometry. For all investigated cases the pressure level of the second ramp is increased significantly compared to the inviscid solution. This level is increased for installed side walls due to the prevented spillage flow. The separation length is increased for increased wall temperature and constant total or free stream temperature and for decreased total temperature for constant wall temperature ratio.

The obtained results indicate clearly the importance to reproduce all flow similarity parameters of a scramjet inlet being

- Mach number,
- Reynolds number,
- wall temperature and
- total temperature.

For the decision if side walls for the scramjet inlet's outer compression should be employ preventing spillage flow, a trade-off study has to consider following issues. First, the afore mentioned side wall advantage of preventing spillage and with it increasing mass flow and the disadvantage of increased drag due to the increased flow wetted area has to be taken into account. Second, the side walls add an additional heat load to the ramp geometry due to the corner flow and a complex three-dimensional flow field, but on the other hand increase the compression of the flow.

Finally, these side wall effects on the flow field are scaled with the inlet width to the other inlet dimensions so that for an increased width the side wall effects are less pronounced.

5. REFERENCE

[1] Weigand, B., Gaisbauer, U., Reinartz, B., Kau, H.-P., Schröder, W.: Das Graduiertenkolleg 1095/1: „Aero-Thermodynamische Auslegung eines Scramjet-Antriebssystems für zukünftige Raumtransport-systeme“, DLRK Jahrestagung 2006, Darmstadt, 2006

[2] Gaisbauer, U., Weigand, B., Reinartz, B.: Research Training Group GRK 1095/1: „Aero-Thermodynamik Design of a Scramjet Propulsion System“, ISABE Conference 2007, Beijing, China, 2007

[3] Gaisbauer, U., Weigand, B.: Research Training Group GRK 1095/1: „The Aero-Thermodynamic Design of a Scramjet Propulsion System“ – an overview, ICMAR Conference 2008, Novosibirsk, Russia, 2008

[4] Neuenhahn, T., Olivier, H.: Influence of the wall temperature and the entropy layer effects on double wedge shock wave/boundary layer interactions, AIAA Paper 2006-8136, 14th AIAA/AHI Space Planes Conference and Hypersonic Systems Conference, Canberra, Australia, 2006

[5] Neuenhahn, T., Olivier, H.: Numerical study of wall temperature and entropy layer effects on transitional double wedge shock wave/boundary layer interactions, 26th International Symposium on Shock Waves, Goettingen, Germany, 2007

[6] Anderson J. D.: Hypersonic and high temperature gas dynamics, AIAA, 2000, ISBN 1-56347-459-X

[7] Grönig, H., Olivier, H.: Experimental hypersonic flow research in Europe, JSME Int. J., Series B, Vol. 41, No.2, 1998, pp. 397- 407

[8] Olivier, H., Jiang, Z., Yu, HR., Lu, F.: Detonation-driven shock tubes and tunnels, Advanced Hypersonic Test Facilities, edited by F. Lu, D. Marren, Progress in Astronautics and Aeronautics, AIAA Inc., Vol. 198, 2002, pp. 135-203

[9] Olivier, H., Zechner, M.: Slender conical nozzle, MSTP Progress Report, HT-SF-E34-731-RWTH, Shock Wave Laboratory, RWTH Aachen University, 1996

[10] Lewis, J.E., Kubota, T., Lees, T.: Experimental investigation of supersonic laminar, two-dimensional boundary layer separation in a compression corner with and without cooling, AIAA Journal, Vol. 6, No. 1, 1968, pp. 7-14

[11] Olivier, H., Grönig, H.: Instrumentation techniques of the Aachen shock tunnel TH2, Proc. of the 16th Int. Congress on Instrumentation in Aerospace Simulation Facilities, Wright-Patterson Air Force Base, 95-CH3482-7,1.1-1.16, Dayton/Ohio,1995

[12] Delery, J., Marvin, J.G.: Shock-wave boundary layer interactions, AGARD Report 761, NATO, Brussels, 1989

[13] Van Driest, E.R.: Investigation of laminar boundary layer in compressible fluids using the Crocco method, TN 2597,1952, NACA

[14] Kreins, A.F.: Heat flux distribution and flow field investigation in distributed hypersonic boundary layers on flat plates, DLR-Forschungsbericht 94-03, published in German, 1994, ISSN 0939-2963

[15] Eckert, E.R.G.: Engineering relations for heat transfer and friction in high-velocity laminar and turbulent boundary-layer flow over surfaces with constant pressure and temperature, Trans. of the ASME, Vol. 78, No.6, 1956, p.1273